Pergamon

Polyhedron Vol. 14, No. 10, pp. 1381–1392, 1995

0277–5387/95 $9.50+0.00

0277-5387(94)00387-4

HIGH-VALENT MANGANESE IN POLYOXOTUNGSTATES—1. MANGANESE(IV) KEGGIN DERIVATIVES

XIAO-YAN ZHANG, MICHAEL T. POPE,* MARK R. CHANCE† and GEOFFREY B. JAMESON‡

Department of Chemistry, Georgetown University, Washington, DC 20057–2222, U.S.A.

(*Received* 13 *July* 1994; *accepted* 21 *September* 1994)

Abstract—Aqueous and non-aqueous soluble salts of manganese(IV)-containing Keggin polyoxotungstates $[(XO_4)W_{11}Mn^{IV}O_{36}H_x]^{n-}$ (X = Si, B, and Zn) have been prepared by chemical and electrolytic oxidation of corresponding manganese(II) or manganese(III) anions, and have been characterized by magnetic susceptibilities, ESR and X-ray absorption near-edge spectroscopy (XANES), in addition to conventional elemental and spectroscopic analyses. The crystal structure of dark brown $K_7[(ZnO_4)W_{11}Mn^{IV}O_{36}H]\cdot 19H_2O$ (**I**) was determined by X-ray diffraction and reveals a disordered Keggin anion.

Manganese EXAFS investigation of **I** and the corresponding manganese(II) complex, which contains a terminal Mn^{II}—OH_2 group, strongly indicates that **I** contains Mn^{IV}—OH ($r_{Mn-O} \sim 1.82$ Å) rather than Mn^{IV}=O.

The catalytic activity of polyoxometalates has attracted increased attention in recent years.[1,2] One class of polyoxoanions, comprising Keggin, $[(XO_4)M_{12}O_{36}]^{n-}$, and related species in which a molybdenum or tungsten atom M has been replaced by a transition metal cation, has proved to display many reactive characteristics of metalloporphyrins, with the added advantage of possessing an oxidatively inert "ligand".[3–14] We have shown that manganese derivatives of this type can activate dioxygen,[9] and Hill,[6,7,14] Finke,[12,13] Neumann,[10,11,15] Liu[16] and their co-workers have explored the use of such complexes as epoxidation catalysts with iodosylbenzene or hydrogen peroxide as oxygen donors.

The first manganese-containing polyoxoanions of this type were reported by Weakley and Tourné.[17] Oxidation states II and III are established for manganese in these complexes, but it has been proposed that higher oxidation state(s) must be involved in the catalysis.[7] Manganese(IV), a d^3 species, favours "octahedral" coordination and is well represented in polyoxometalate chemistry as a central heteroatom in molybdate,[18] tungstate,[19] vanadate[20] and niobate[21] matrices. Manganese(IV) with a unique terminal ligand is less common, although not unprecedented, e.g. $[L_2Mn^{IV}_2(OH)_2(\mu\text{-}O)_2][Mn^{II}_3(C_2O_4)_4(OH_2)_2]\cdot 6H_2O$ (L = 1,4,7-triazacyclononane).[22]

According to the literature, oxidation of $[(XO_4)W_{11}MnO_{36}H_2]^{n-}$ does not proceed beyond manganese(III), although we have shown that the trimanganese complex $[(SiO_4)W_9\{Mn(OH_2)\}_3O_{33}]^{10-}$ can be oxidized to the Mn^{III}_3 and Mn^{IV}_3 states.[23] We have therefore reinvestigated the accessibility of higher oxidation states of manganese in "surface" sites of polyoxotungstate anions containing manganese(IV). Subsequent papers will describe di- and tetra-manganese polyoxotungstate complexes, and a comparison of redox and catalytic activities of all the manganese species.

* Author to whom correspondence should be addressed.

† Present address: Department of Physiology and Biophysics, Albert Einstein College of Medicine, Bronx, NY 10461, U.S.A.

‡ Present address: Department of Chemistry and Biochemistry, Massey University, Palmerston North, New Zealand.

EXPERIMENTAL

Syntheses

Potassium undecatungstomangano(II) *phosphate, silicate, borate and zincate* $\{K_5[(PO_4)W_{11}Mn^{II}O_{36}H_2]\cdot 15H_2O$ $(PW_{11}Mn^{II})$, $K_6[(SiO_4)W_{11}Mn^{II}O_{36}H_2]\cdot 21H_2O(SiW_{11}Mn^{II})$, $K_7[(BO_4)W_{11}Mn^{II}O_{36}H_2]\cdot 16H_2O$ $(BW_{11}Mn^{II})$ *and* $K_8[(ZnO_4)W_{11}Mn^{II}O_{36}H_2]\cdot 23H_2O$ $(ZnW_{11}Mn^{II})\}$. These were prepared according to the methods of Weakley and co-workers.[17a,24] The yellow or ochre products were characterized by IR spectroscopy and by oxidation of their aqueous solutions to the corresponding red or orange manganese(III) complexes using $K_2S_2O_8$ (for $PW_{11}Mn^{II}$ and $SiW_{11}Mn^{II}$) or 5% H_2O_2 (for $ZnW_{11}Mn^{II}$ and $BW_{11}Mn^{II}$) as described.[17a] The visible absorption spectra of $XW_{11}Mn^{III}$ agreed with the literature:[17a] λ_{max} (ε), for X = P, 495.0 (252), 507.5 (sh, 247), 526.0 (229), 556.5 (sh, 139), 769.0 nm (br, 13); for X = Si, 490.0 (219), 505.0 (sh, 207), 521.0 (188), 552.5 (sh, 101), 800 nm (br, 11); for X = B, 476.0 (314), 500 (sh, 226), 515.5 (176), 571.5 (sh, 50), 807 nm (br, 27); and for X = Zn, 467.5 (sh, 213), 522 (248), 800 nm (br, 43).

Salts of undecatungstomangano(IV) silicate, borate and zincate, $XW_{11}Mn^{IV}$, were prepared by controlled-potential electrolyses of $XW_{11}Mn^{II}$ solutions or by chemical oxidation. All electrolyses were carried out in a 0.2 M potassium acetate–acetic acid (KOAc–HOAc) buffer, pH 4.7.

Potassium and tetra-n-hexylammonium undecatungstomangano(IV) *zincate.* A solution of 6.2 g potassium salt of $ZnW_{11}Mn^{II}$ in 120 cm^3 buffer was electrolysed at 1.05 V vs SCE (saturated calomel electrode); 2.05 oxidizing equivalents were transferred. Fifteen grams of potassium acetate was added to the solution, which yielded fine brown crystals. The crude product was filtered off and carefully recrystallized from the buffer at 60–65°C and cooled in a refrigerator. The brown crystals were filtered off, washed with a little cold water and dried in air. The yield was about 50%. Found: K, 8.5; Zn, 1.6; W, 59.3; Mn, 1.5; H_2O, 10.0 (750°C). Calc. for $K_7[(ZnO_4)W_{11}Mn^{IV}O_{36}H]\cdot 19H_2O$: K, 8.1; Zn, 1.9; W, 59.5; Mn, 1.6; H_2O, 10.1%.

Addition of solid tetra-n-hexylammonium (THA) chloride to an electrolysed solution as described above resulted in the precipitation of a sticky brown solid, which was separated, redissolved in acetonitrile and reprecipitated with water. Found: C, 35.9; N, 2.0; H, 6.7; W, 35.3; Mn, 1.0; Zn, 1.1. Calc. for $[(C_6H_{13})_4N]_7[(ZnO_4)W_{11}Mn^{IV}O_{36}H]\cdot 21H_2O\cdot CH_3CN$: C, 35.7; N, 2.0; H, 6.5; W, 35.4; Mn, 1.0; Zn, 1.1%.

Caesium and tetra-n-butylammonium undecatungstomangano(IV) *borate.* A solution of 4.2 g potassium salt of $BW_{11}Mn^{II}$ in 60 cm^3 buffer was electrolysed at 1.2 V vs SCE. After 2.3 equivalents were transferred, 2.5 g $CsNO_3$ was added to the reddish-brown solution, and fine reddish-brown crystals were formed. The solid was filtered off and recrystallized from hot water (60°C), then cooled in a refrigerator. Reddish-brown crystals were obtained, filtered off, washed with cold water and dried in air. The yield was about 60%. Found: K, 0.4; Cs, 19.1; W, 54.3; Mn, 1.0; H_2O, 5.3 (800°C). Calc. for $Cs_{5.4}K_{0.6}[(BO_4)W_{11}Mn^{IV}O_{36}H]\cdot 15H_2O$: K, 0.6; Cs, 19.2; W, 54.1; Mn, 1.5; H_2O, 7.2%.

Addition of solid tetra-n-butylammonium (TBA) nitrate to an electrolysed solution as described above gave a brown precipitate, which was purified from acetonitrile–water solution as described above, and gave a reddish-brown powder. Found: C, 24.3; N, 1.9; H, 4.7; W, 48.1; Mn, 1.2; B, 0.10. Calc. for $[(C_4H_9)_4N]_{5.3}[(BO_4)W_{11}Mn^{IV}O_{36}H_{0.7}]\cdot 10H_2O\cdot 0.5CH_3CN$: C, 24.2; N, 1.9; H, 4.5; W, 48.1; Mn, 1.3; B, 0.3%.

Caesium and tetra-n-butylammonium undecatungstomangano(IV) *silicate.* A solution of 6.2 g potassium salt of $SiW_{11}Mn^{II}$ in 60 cm^3 buffer was electrolysed at 1.2 V vs SCE. After the transfer of 2.3 equivalents, 3.0 g $CsNO_3$ was added to the solution and the resulting precipitate was filtered off, recrystallized from 0.05 M KOAc–HOAc, pH 4.7, at 70°C and cooled in a refrigerator. The brown powder was filtered off, washed with cold water and dried in air. The yield was about 75%. Found: K, 0.3; Cs, 17.5; W, 55.1; Mn, 1.3; H_2O, 7.3 (800°C). Calc. for $Cs_{4.8}K_{0.2}[(SiO_4)W_{11}Mn^{IV}O_{36}H]\cdot 14.5H_2O$: K, 0.2; Cs, 17.5; W, 55.5; Mn, 1.5; H_2O, 7.2%.

Addition of tetra-n-butylammonium nitrate to the electrolysed solution as described above gave a brown solid, which was purified from H_2O–CH_3CN solution as described above.

Found: C, 22.4; N, 1.8; H, 4.2; W, 46.7; Mn, 1.2; Si, 0.6. Calc. for $[(C_4H_9)_4N]_5[(SiO_4)W_{11}Mn^{IV}O_{36}H]\cdot 18H_2O\cdot 0.5CH_3CN$: C, 22.3; N, 1.8; H, 4.2; W, 47.3; Mn, 1.3; Si, 0.7%.

Samples of the above three manganese(IV) complexes were also prepared by oxidation with $K_2S_2O_8$. Solutions of 5 g $XW_{11}Mn^{II}$ and 5 g $K_2S_2O_8$ in 15 cm^3 deionized water were heated to about 90°C with stirring. After the colour of the solution changed from yellow to brown or reddish-brown, the solutions were cooled to room temperature and the excess $K_2S_2O_8$ was filtered out. Addition of 3.0 g $CsNO_3$ to the filtrates gave brown solids which were recrystallized from the acetate buffer. Yields were 75–85%.

When $XW_{11}Mn$ salts are converted to organic solvent soluble derivatives by precipitation as tetra-

n-butylammonium salts (X = P, Si) or by extraction into hexanes as tetra-n-heptylammonium salts (X = B, Zn), the zinc and boron derivatives are spontaneously air-oxidized to the manganese(III) state.[9] Treatment of solutions of $ZnW_{11}Mn^{III}$, $BW_{11}Mn^{III}$ and $SiW_{11}Mn^{III}$ in CCl_2H_2–CH_3CN (1 : 1) with iodosylbenzene rapidly (*ca* 2 min) generated brown solutions with electronic absorption and EPR spectra characteristic of the manganese(IV) derivatives. The corresponding reaction with $PW_{11}Mn^{II}$ led only to pink $PW_{11}Mn^{III}$.

The manganese(IV) heteropolyanions are reduced by dilute hydrogen peroxide, and this may account for the fact these substances were not identified earlier. Addition of a drop of 3% H_2O_2 to an aqueous solution of brown $XW_{11}Mn^{IV}$ leads to the formation of pink or orange $XW_{11}Mn^{III}$. The rates of reduction are dependent upon X: Si (colour or visible spectrum change apparent within 1 min) > Zn (3 min) > B (20 min). Consequently, if H_2O_2 is employed to oxidize $XW_{11}Mn^{II}$ only, the manganese(III) complexes are produced, except in one case. When 0.3 g of the potassium salt of $ZnW_{11}Mn^{II}$ was dissolved in 1 cm^3 15% H_2O_2 a brown solution was generated within 3 min. After 30 min the colour had changed to pink, and the visible spectrum corresponded to that of $ZnW_{11}Mn^{III}$. Attempts to separate the brown intermediate, presumed to be $ZnW_{11}Mn^{IV}$, were unsuccessful. Treatment of solutions of $BW_{11}Mn^{II}$ and $SiW_{11}Mn^{II}$ with more concentrated H_2O_2 yielded only the manganese(III) complexes or bleached solutions that may indicate polyanion decomposition or perhaps the existence of higher oxidation states of manganese.

X-ray diffraction

Single crystals of $K_7[(ZnO_4)W_{11}Mn^{IV}O_{36}H]\cdot 19H_2O$ were obtained from KOAc–HOAc (0.2 M, pH 4.7) buffer solution.

Intensity data were collected on a modified Picker diffractometer. The parameters and crystal data are listed in Table 1. Tungsten atom positions were chosen from another structure of the same structure type and confirmed by direct methods and Patterson function. Other atoms were located by difference Fourier syntheses alternating with cycles of full-matrix least-squares refinement. An empirical absorption correction (DIFABS) was applied when all non-hydrogen atoms had been located.

The 1/12 Mn^{IV} and 11/12 W^{VI} at each tungsten site were assumed to have the same positional and thermal parameters. Other models, in which manganese(IV) and tungsten(VI) have different positional and/or different thermal parameters, do not give better R values. Before anisotropic refinement, the R values were $R_1 = 4.38$ and $R_2 = 5.93$. With anisotropic thermal parameters only for tungsten, the structure was refined to $R_1 = 0.030$ and $R_2 = 0.040$ using 314 data with $I > 5\sigma_1$ and weighting factor $W = \sigma^2(F_0^2) = \sigma^2_{\text{counting}} + (pF_0^2)^2$. From analysis of $|F_0|$ vs $|F_c|$, several intense low angle data affected by extinction (e.g. the 444 reflection) were deleted. In the final cycle of refinement, W and K were allowed to refine anisotropically and led to $R_1 = 0.028$ and $R_2 = 0.036$ with 309 observed data.

Table 1. Crystal data for $K_7[(ZnO_4)W_{11}Mn^{IV}O_{36}H]\cdot 19H_2O$ and data collection procedures

Formula weight	3244
Space group	*Fm3m*
$a = b = c$ (Å)	21.434 (47)
Crystal size (mm)	$0.12 \times 0.12 \times 0.06$
D_{calc} (g cm^{-3})	4.38
D_{obs} (g cm^{-3})	4.31
Z	8
Crystal colour	brown
Linear abs. coeff. (cm^{-1})	274.9
Shape	block
DIFABS absorption correction	
Transmission factors (%)[a]	0.77–1.46
Scan type	θ–2θ
Scan speed (° min^{-1})	2.0
Sin θ/λ limits ($Å^{-1}$)	0.04–0.65
Total no. reflections	3044
No. of unique data	628 [$R_{av}(F) = 0.04$]
No. of unique data with $F_0^2 > 5\sigma F_0^2$	313
Final least-squares refinement	
Reflections used	$I > 5\sigma_1$
Sin θ/λ limits ($Å^{-1}$)	0.10–0.65
p($w = K/[\sigma^2_{\text{count}} + (\text{pI})^2]$)	0.04
Data/parameter	309/30
Extinction coeff.	not refined
Final $R(F)$ [$R_w(F)$]	0.028 (0.036)

[a] DIFABS absorption correction factors.

EXAFS and XANES

Data collection. Data were collected at the National Synchrotron Light Source, Brookhaven National Laboratory, on beam lines X-9A or X-10C. All experiments were carried out at 220–155 K, and the sample temperature was maintained by flowing cooled nitrogen gas through a low-temperature cryostat, as described previously.[25] The samples were diluted with Al_2O_3 powder to 0.3% in manganese. X-ray edge data with 3 eV resolution were recorded at a specific energy for 2 s in 0.5 eV

increments from 20 eV below the manganese K-edge (6537 eV) to 50 eV above the edge. EXAFS data were collected with 2 eV increments from 30 eV below the edge to 30 eV above the edge, and 3 eV increments from 30 to 600 eV above the edge under the same resolution. The exposed area of the sample was 10 mm^2.

The known structures, pyrolusite (MnO_2, kindly supplied by the Smithsonian Institution), $Na_2K_6[Mn^{IV}W_6O_{24}]\cdot nH_2O$ [r(Mn—O) = 1.931(7) Å[19]] and $Na_7[Mn^{IV}(HIO_6)(H_2IO_6)_2]\cdot 18H_2O$ [r(Mn—O) = 1.896(3) Å[26]] were used as standard compounds.

Manganese K_α fluorescence was detected with a zinc sulphide-coated photomultiplier tube (PMT) and incident photon scattering was rejected by a chromium filter. Output signals were amplified with a Keithley amplifier, converted to frequency and counted in a scaler interfaced to a computer via CAMAC. For reference signals, mylar tape was mounted at a 45° angle to the X-ray beam to scatter photons counted by a similar PMT positioned perpendicular to the X-ray beam. A transmission spectrum of a standard manganese foil was determined simultaneously using a third PMT in a similar geometry to the reference.[27]

Data analysis and error. Data were processed and analysed using the University of Washington EXAFS package on an 8700 VAX computer.

For each sample, eight scans were averaged for EXAFS data and the background was normalized by linear subtraction. The fluorescence amplitude was multiplied by k^3, where $k = [(E-E_0)^{1/2}]/C$ and $C = h/[(2\pi)(2m_e)^{1/2}]$. This cancels the approximate $1/k^3$ dependence of the data and equalizes the contributions at high and low k. The data for $ZnW_{11}Mn^{IV}$ and $ZnW_{11}Mn^{II}$ plotted as a function of k are shown in Fig. 1.

The different ligand shells can be isolated by a Fourier transform of the data, as shown in Fig. 2. The first shell ligands have the highest Fourier magnitude; this contribution can be isolated and, after back-transformation, can be compared with known manganese models that have been treated in the same manner. Figure 3 shows the back-transformation of the measured $ZnW_{11}Mn^{IV}$ and its best fit calculation.

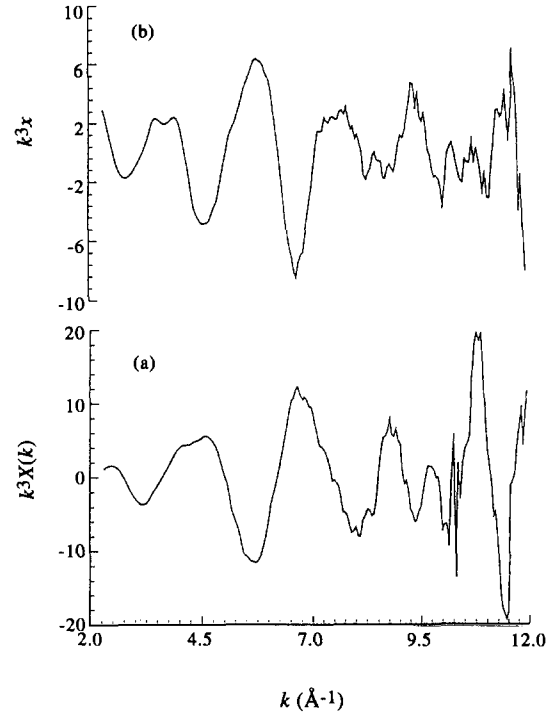

Fig. 1. EXAFS of: (a) $K_7[(ZnO_4)W_{11}Mn^{IV}O_{36}H]\cdot 19H_2O$ and (b) $K_8[(ZnO_4)W_{11}Mn^{II}O_{36}H_2]\cdot 23H_2O$. Fluorescence amplitude normalized to one absorbing atom and multiplied by k^3 vs k.

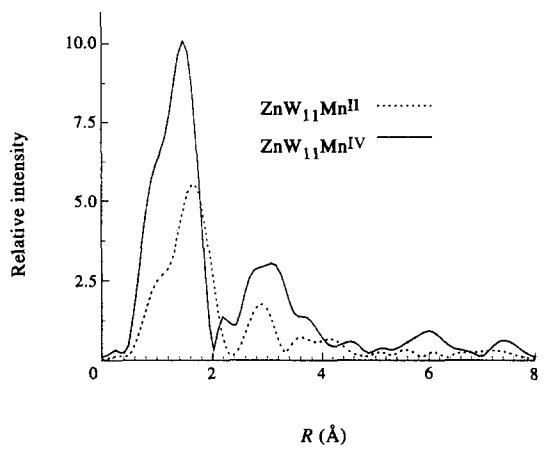

Fig. 2. Fourier transform of EXAFS data of $K_7[(ZnO_4)W_{11}Mn^{IV}O_{36}H]\cdot 19H_2O$ and $K_8[(ZnO_4)W_{11}Mn^{II}O_{36}H_2]\cdot 23H_2O$.

Cyclic voltammetry and controlled potential electrolyses

Cyclic voltammograms (CVs) were recorded on a BAS 100A electrochemical analyser with glassy carbon as the working electrode, a platinum wire as the counter electrode, an Ag/AgCl reference electrode, and sweep rate 20 mV min^{-1}. Solutions were 5.0 mM in heteropolyanion in 0.2 M acetate buffer, pH 3.5–6.0. Controlled potential electrolysis was carried out using a Brinkman Wenking Potentiostat (Model 70TST) with a Koslow Scientific Co. digital coulometer (Model 541), graphite cloth (National Electrical Carbon Corporation) working electrode, platinum wire counter electrode and saturated calomel reference electrode at room temperature. The

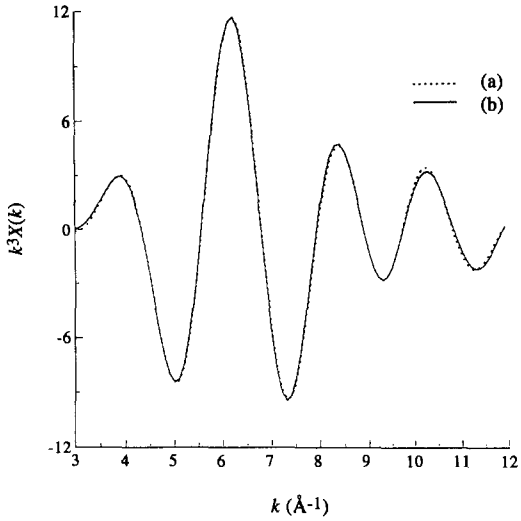

Fig. 3. (a) First-shell-filtered back-transformed EXAFS spectrum of $K_7[(ZnO_4)W_{11}Mn^{IV}O_{36}H]\cdot 19H_2O$. (b) Fitted spectrum using parameters listed in text.

counter electrode was separated from the bulk solution by a fritted glass bridge. The potentials for reduction and oxidation were chosen from the CV.

Other measurements

ESR spectra were measured on a Varian E-4 spectrometer with a TM_{110} rectangular cavity. The radical DPPH ($g = 2.004$) was used to determine the microwave frequency. An immersion Dewar with liquid N_2 was used to record spectra at 77 K.

Magnetic susceptibilities were measured[28a] between 80 and 295 K on a computer-controlled Faraday system, which consists of a Cahn 2000 microbalance, Applied Magnetic electromagnet, Lake Shore Cryotronics temperature controller, platinum-resistance thermometer and Abbess instrument cryostat. A data translation A/D board and AT computer were used to monitor the microbalance output and temperature readings. The instrument was calibrated with $HgCo(NCS)_4$.[28b] The raw data were corrected for the susceptibility of the holder and the diamagnetism of heteropolyanions (-500×10^{-6} c.g.s. units),[29] and converted into molar susceptibilities from which the magnetic moments were calculated as $\mu = 2.828 (X_M T)^{1/2}$.

Solid state IR spectra were recorded on a Nicolet 170SX FTIR spectrophotometer using KBr pellets. UV–vis spectra were measured on an 8451A HP diode array spectrophotometer with a 1-cm quartz cell. Elemental analyses were performed by the E+R Microanalytical Laboratory (Corona, New York). All chemicals used were analytical grade or higher and were not further purified.

RESULTS AND DISCUSSION

Electrochemistry

Cyclic voltammograms of $XW_{11}Mn^{II}$ (X = Zn, B, Si and P) are shown in Fig. 4. The single quasi-reversible feature for $PW_{11}Mn^{II}$ corresponds to a one-electron process as shown by controlled potential oxidation at 1.00 V (0.97 equiv. mol^{-1}) and subsequent re-reduction at 0.30 V (0.95 equiv. mol^{-1}). The visible spectrum of the oxidized solution confirmed the formation of $PW_{11}Mn^{III}$. The effective redox potential (0.72 V vs Ag/AgCl), determined from the average of the anodic and cathodic peak potentials ($\Delta E = 80$–170 mV), is independent of pH from 3.5 to 6.5.

The CV of $SiW_{11}Mn^{II}$ shows two* oxidation processes. Electrolysis of a solution containing 339 mg

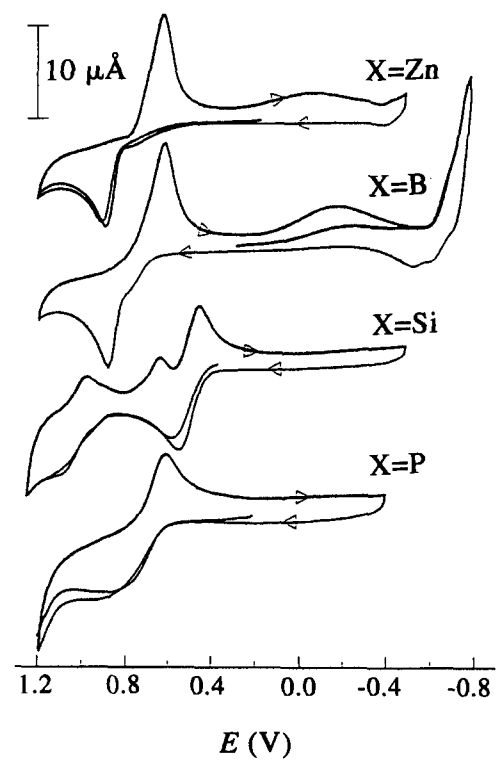

Fig. 4. Cyclic voltammograms of 5.0 mM potassium salts of $XW_{11}Mn^{II}$ (X = Zn, B, Si and P) in 0.2 M KOAc–HOAc at pH 4.8.

* The CV of $SiW_{11}Mn^{II}$, but not those of $SiW_{11}Mn^{III}$ and $SiW_{11}Mn^{IV}$ generated by electrolysis as described, shows an additional cathodic peak at 0.65 V. We have been unable to discover an unambiguous explanation for this peak.

potassium salt of $SiW_{11}Mn^{II}$ in 20 cm^3 pH 4.8 buffer was conducted in two stages. At 0.80 V, 1.08 equivalents were transferred and the resulting red solution had an absorption spectrum corresponding to that of $SiW_{11}Mn^{III}$. When the potential was increased to 1.18 V and the solution spectrum was monitored by the loss of the peak at 490 nm, an additional 1.2 equivalents were transferred and the solution became brown. The caesium salt of $SiW_{11}Mn^{IV}$ was isolated from this solution as described in the Experimental section. Electrolysis of a solution of this salt (180 mg in 12 cm^3 buffer) was carried out at 0.5 V (0.98 equiv.) and subsequently at −0.2 V (0.97 equiv.) in two steps, consistent with the CV of $XW_{11}Mn^{IV}$ shown in Fig. 5. The products of electrolysis, $SiW_{11}Mn^{III}$ and $SiW_{11}Mn^{II}$, were identified by UV–vis spectroscopy and CV.

The CVs of $BW_{11}Mn^{II}$ and $ZnW_{11}Mn^{II}$ show one major anodic peak and two cathodic peaks. Electrolysis of $BW_{11}Mn^{II}$ (5.0 g in 50 cm^3 buffer) at 1.20 V caused colour changes from yellow–orange to orange to reddish-brown. After passage of one equivalent per mole, the orange solution showed the characteristic spectrum of $BW_{11}Mn^{III}$. Continued electrolysis until the peak at 476.0 nm had disappeared took about 6 h and resulted in transfer of 2.3 equivalents overall. The caesium salt of $BW_{11}Mn^{IV}$ was isolated from this solution as described in the Experimental section. Electrolysis of this salt solution (234 mg in 12 cm^3 buffer) was carried out at $E = 0.0$ V (1.06 equiv.) and subsequently at $E = -0.40$ V (0.95 equiv.). The products of the electrolyses were identified as $BW_{11}Mn^{III}$ and $BW_{11}Mn^{II}$ respectively by UV–vis spectroscopy and CV.

Electrolysis of $ZnW_{11}Mn^{II}$ (266 mg in 20 cm^3 buffer) at 1.05 V caused colour changes from yellow to pink to reddish-brown. After one equivalent had been transferred, the UV–vis spectrum of the pink solution was the same as that for $ZnW_{11}Mn^{III}$. The electrolysis was complete within 30 min, and 2.05 equivalents were transferred overall. The potassium

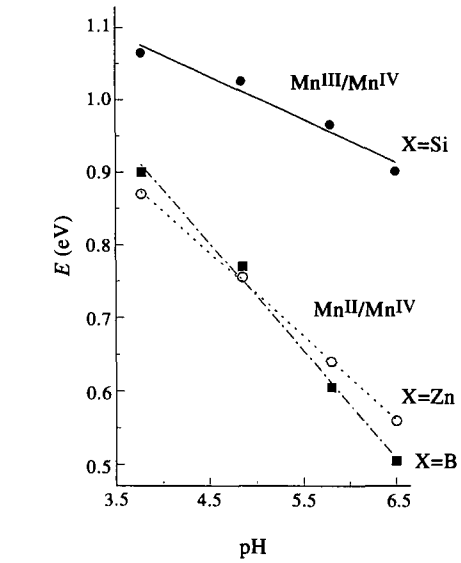

Fig. 6. Variation of voltammetric redox potentials, $\frac{1}{2}(E_{pc} + E_{pa})$, of $XW_{11}Mn^{II}$ (X = Zn, B and Si) with pH. The Mn^{II}/Mn^{III} potential for $SiW_{11}Mn$ is invariant. For experimental details, see text.

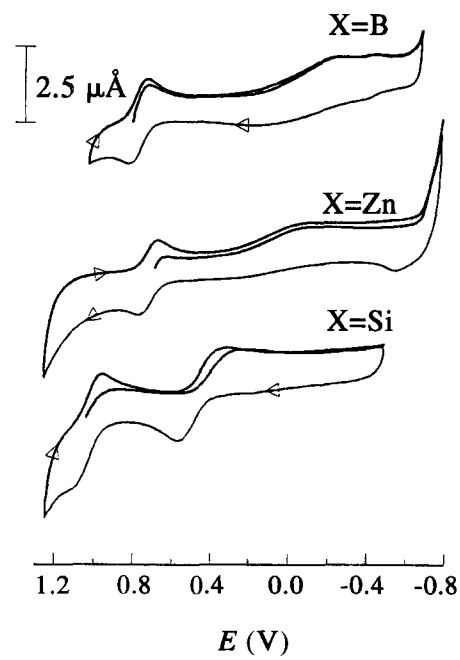

Fig. 5. Cyclic voltammograms of 5.0 mM caesium or potassium salts of $XW_{11}Mn^{IV}$ (X = Zn, B and Si) in 0.2 M KOAc–HOAc at pH 4.8.

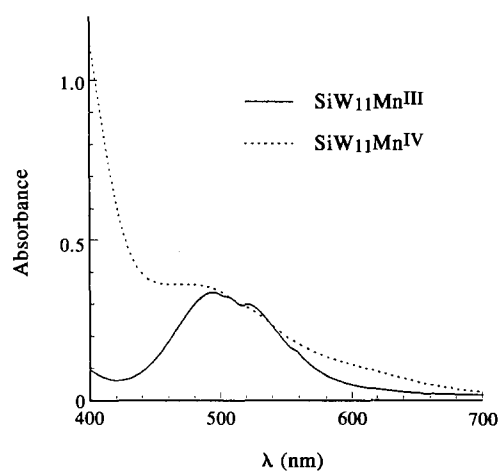

Fig. 7. UV–vis spectra of 0.9 mM caesium salts of $SiW_{11}Mn^{IV}$ and $SiW_{11}Mn^{III}$ (0.9 mM $SiW_{11}Mn^{IV}$ in 2 mM H_2O_2).

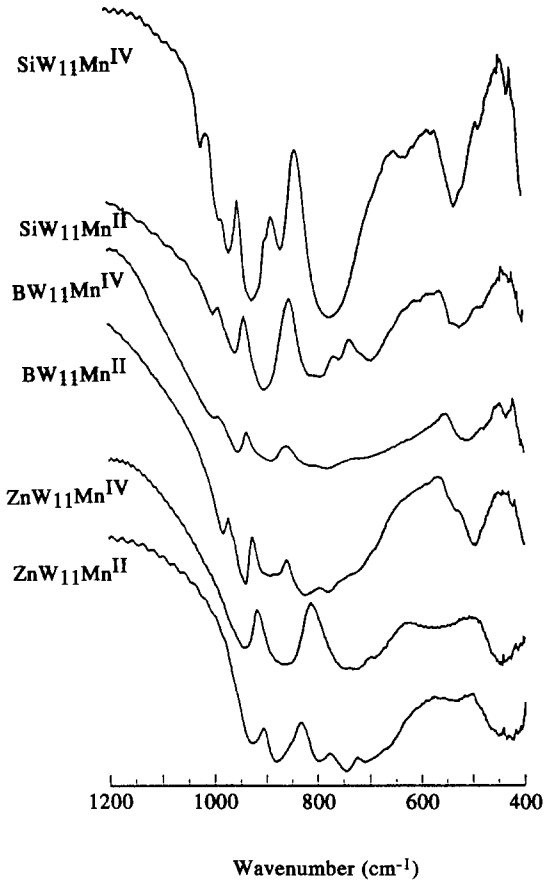

Fig. 8. IR spectra of potassium or caesium salts of $XW_{11}Mn^{II}$ and $XW_{11}Mn^{IV}$ (X = Zn, B and Si).

salt of $ZnW_{11}Mn^{IV}$ was isolated from this solution as described in the Experimental section. Electrolysis of a solution of this salt (127 mg in 12 cm^3 buffer) was carried out at $E = 0.40$ V (0.98 equiv.) and subsequently at -0.2 V (0.95 equiv.) according to CV. The products of electrolyses ($ZnW_{11}Mn^{III}$ and $ZnW_{11}Mn^{II}$) were identified by UV–vis spectroscopy and CV.

The effective redox potentials of Mn^{II}–Mn^{III} in $SiW_{11}Mn^{II}$ ($E = 0.50$ V vs Ag/AgCl with ΔE = 70–150 mV) and $PW_{11}Mn^{II}$ ($E = 0.71$ V vs Ag/AgCl with ΔE = 70–170 mV) are pH-independent. However, the effective redox potentials of Mn^{III}–Mn^{IV} are pH-dependent, as shown in Fig. 6. Since both redox processes are quasi-reversible at best, we cannot determine the number of protons accompanying electron transfer with certainty from these data.

Spectroscopy and magnetochemistry

The UV–vis spectral features of $XW_{11}Mn^{IV}$ cannot be located very well, because the charge transfer bands for O → W and O → Mn^{IV} overlap and are much more intense than the *d–d* bands of manganese(IV). In order to compare $XW_{11}Mn^{IV}$ with related $XW_{11}Mn^{III}$, the UV–vis spectra were recorded at the same concentration (see Fig. 7 for example).

From the comparison, the $XW_{11}Mn^{IV}$ anions have O → Mn^{IV} charge transfer bands below 400 nm and *d–d* transitions ($^4A_{2g} \rightarrow {}^4T_{2g}$) around 450–500 nm, like the known manganese(IV) complex, $Na_7[Mn^{IV}(HIO_6)(H_2IO_6)_2] \cdot 18H_2O$.[26] IR spectra of $XW_{11}Mn^{IV}$ and $XW_{11}Mn^{II}$ are shown in Fig. 8.

The X-band ESR spectra of powder and frozen acetonitrile solutions of $XW_{11}Mn^{IV}$ are shown in Fig. 9. The ESR spectrum of manganese(IV) can be treated theoretically by the method[30] developed for Chromium(III) and known manganese(IV).[31] The X-band spectrum of a d^3 ion depends on the electronic symmetry. In an axial field ($E/D = 0$),

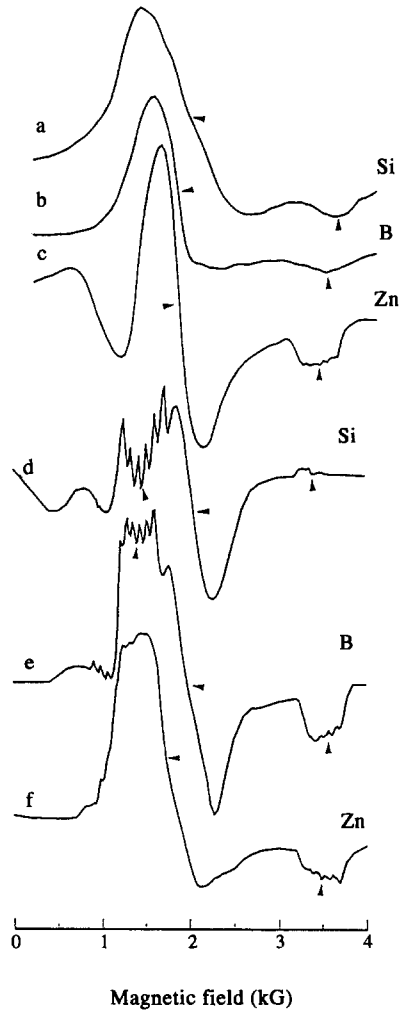

Fig. 9. X-band EPR spectra of $XW_{11}Mn^{IV}$ (X = Zn, B and Si) at 77 K. (a–c) Polycrystalline samples of potassium or caesium salts. (d–f) Samples of NR_4^+ salts recorded in frozen solution (CH_2Cl_2–CH_3CH, 1 : 1). *g*-values were evaluated at the positions indicated.

the spectrum depends on the magnitude of the zero-field splitting parameters. When D is much larger than hv, the feature at $g \approx 2$ should be very small and that at $g \approx 4$ should be dominant. In rhombic symmetry, an additional absorptive feature at $g > 4$ appears; its exact position depends upon the rhombicity. All spectra of $XW_{11}Mn^{IV}$ show more intense features at $g \approx 4$ and weak features at $g \approx 2$. This indicates that $D \gg hv$, and is consistent with the long axial Mn^{IV}—O(X) bond in the Keggin structure. All g values and the hyperfine splitting by manganese nuclei (^{55}Mn, $I = 5/2$) are summarized in Table 2.

The variable temperature magnetic susceptibilities follow the Curie–Weiss law, and the parameters are listed in Table 3. The magnetic moments of manganese(IV) compounds are close to the d^3 spin-only value (3.87 B.M.).

Crystal structure

X-ray diffraction studies confirm that $K_7[(ZnO_4)W_{11}Mn^{IV}O_{36}H] \cdot 19H_2O$ has the Keggin structure. The space group is $Fm3m$, the same as for other NH_4^+ or K^+ salts of XZW_{11} heteropolyanions with charges of -7 and -8.[32] The heteropolyanions have $43m$ (T_d) symmetry and each anion is inverted with respect to its neighbours.

Table 2. ESR parameters of manganese(IV) compounds

Compound	g_1	g_2	g_3
$K_7[(ZnO_4)W_{11}Mn^{IV}O_{36}H] \cdot 19H_2O$	1.94 (100[a])	3.73	
$Cs_{5.4}K_{0.6}[(BO_4)W_{11}Mn^{IV}O_{36}H] \cdot 11H_2O$	1.90	3.72	
$Cs_{4.8}K_{0.2}[(SiO_4)[W_{11}Mn^{IV}O_{36}H] \cdot 14.5H_2O$	1.84	3.22	
$THA_7[(ZnO_4)W_{11}Mn^{IV}O_{36}H] \cdot 21H_2O \cdot CH_3CN$	1.90	3.80	
$TBA_{5.3}H_{0.7}[(BO_4)W_{11}Mn^{IV}O_{36}H] \cdot 10H_2O \cdot 0.5CH_3CN$	1.90 (100)	3.31	4.69 (99)
$TBA_5[(SiO_4)W_{11}Mn^{IV}O_{36}H] \cdot 18H_2O \cdot 0.5CH_3CN$	1.90	3.23	4.47 (99)

[a] Manganese hyperfine coupling (G).

Table 3. Magnetic moments and Weiss constants[a]

Compound	μ_{eff} (B.M.)	θ (K)
$K_7[(ZnO_4)W_{11}Mn^{IV}O_{36}H] \cdot 19H_2O$	4.09	1.2 (2)
$Cs_{5.4}K_{0.6}[(BO_4)W_{11}Mn^{IV}O_{36}H] \cdot 15H_2O$	3.61	−1.6 (2)
$Cs_{4.8}K_{0.2}[(SiO_4)W_{11}Mn^{IV}O_{36}H] \cdot 14.5H_2O$	3.95	−2.9 (2)

[a] Temperature range 77–290 K.

Table 4. Selected bond lengths (Å) and bond angles (°) of $K_7[(ZnO_4)W_{11}Mn^{IV}O_{36}H] \cdot 19H_2O$[a]

Zn—O(1)	1.866 (7)	W—O(1)	2.191 (8)
W—O(2)	1.725 (7)	W—O(3)	1.910 (9)
W—O(4)	1.970 (9)	K(1)—O(3)	2.87 (1)
K(1)—O(4)	2.88 (1)	K(2)—O(W1)	2.90 (1)
K(2)—O(2)	2.81 (1)		
O(3)—K(1)—O(3)	180.0 (0)	O(4)—K(1)—O(4)	180.0 (0)
O(3)—K(1)—O(3)	115.9 (4)	O(4)—K(1)—O(4)	80.7 (4)
O(3)—K(1)—O(3)	64.1 (4)	O(4)—K(1)—O(4)	99.3 (4)
O(3)—K(1)—O(4)	56.7 (2)	O(3)—K(1)—O(4)	123.3 (2)
O(2)—K(2)—O(2)	73.8 (4)	O(2)—K(2)—O(2)	116.2 (6)
O(2)—K(2)—O(W1)	81.2 (3)	O(2)—K(2)—O(W1)	142.9 (1)
O(W1)—K(2)—O(W1)	68.1 (3)	O(W1)—K(2)—O(W1)	104.8 (5)

[a] Numbers in parentheses are estimated standard deviations in the least significant digits.

Two types of potassium (total of six potassiums per heteropolyanion) and four types of water (total of 14 H_2O per heteropolyanion) were found. Selected bond angles and bond lengths are listed in Table 4.

As described above, manganese(IV) is disordered over all tungsten positions and the manganese environment cannot be confirmed. However, the type of terminal ligand (hydroxo or oxo) is very pertinent to the redox activity of these heteropolyanions. EXAFS was used to determine the Mn—O bond lengths.

EXAFS and XANES

Data were collected for $Na_2K_6[Mn^{IV}W_6O_{24}]\cdot nH_2O$, $Na_7[Mn^{IV}(HIO_6)(H_2IO_6)_2]\cdot 18H_2O$ and the potassium salts of $ZnW_{11}Mn^{IV}$ and $ZnW_{11}Mn^{II}$. The periodate complex has previously been studied by EXAFS by Levason *et al.*,[26] but the present results are, to our knowledge, the first to be reported for manganese in heteropolyanions. Based on the periodate complex as a model, the data for $[MnW_6O_{24}]^{8-}$ (using k = 3.5–10, with a Fourier filter width of 1.0 Å from 1.0 to 2.0 Å and 0.4 Å tailing at each end) were best fitted to yield r(Mn—O) = 1.93 Å, n = 7.10, $\Delta\sigma^2 = 0.8\times10^{-3}$ Å^2 and ΔE = 1.0 eV, where n is the number of scatterers, and $\Delta\sigma^2$, ΔE are the changes in the Debye–Waller factor and absorption edge energy, respectively, relative to the model compound. The bond distance is in excellent agreement with that determined by crystallography [1.931(7) Å]. We attribute the high value for n (there are of course only six oxygens surrounding the manganese atom) to focussing effects caused by the second shell of six heavy (tungsten) scatterers.[33] Analysis of the data for $ZnW_{11}Mn^{II}$ (using k = 3–9.5, with a Fourier filter of 1.2 Å full width from 0.7 to 1.9 Å) led to r(Mn—O) = 2.13 Å, n = 7.13, $\Delta\sigma^2 = 6.9\times10^{-3}$ Å^2 and ΔE = 1.0 eV. The focussing effect shows clearly with n = 7.13; the manganese atom in this complex is surrounded by at least three types of nearest neighbours: an oxygen bridging manganese and zinc, four oxygens bridging manganese and tungsten, and a terminal water ligand. The observed bond length of 2.13 Å is a reasonable average value, compared with a value of 2.23 Å based on the ionic radius of Mn^{2+} (0.97 Å) in six-fold coordination and O^{2-} (1.26 Å).[34]

We wish to discriminate between the different Mn—O bond lengths in $ZnW_{11}Mn^{IV}$ in order to identify the terminal ligand (O^{2-}, OH^- or H_2O). Analysis of the data for $ZnW_{11}Mn^{IV}$ (using k from 3 to 12 with a Fourier filter of 1.15 Å full width from 0.65 to 1.80 Å without tailing) with fixed n = 6 (we do not understand why the focussing effects

Table 5. EXAFS fitting results for $K_7[(ZnO_4)W_{11}Mn^{IV}O_{36}H]\cdot 19H_2O$

Model	N^a	r (Mn—O) (Å)^b	$\Delta\sigma^2$ (Å$^2\times10^{-3}$)^c	ΔE_0 (eV)^d	R^{2e}
One[f]	6	1.87	−0.41	4.0	2.27
A	1	1.82	−4.8	8.0	1.52
	5	1.90	0.10	2.0	1.52
B	1	2.02	−2.3	−7.0	1.14
	5	1.87	−1.6	3.0	1.14
C	2	1.84	−3.3	8.0	1.39
	4	1.92	0.50	0.0	1.39
D	2	1.98	−0.56	−4.0	1.19
	4	1.86	−2.3	4.0	1.19
E	1	1.82	8.7	6.0	0.95
	1	2.02	−5.8	−8.0	0.95
	4	1.86	−3.6	6.0	0.95

[a] N, number of scatterers.
[b] r, average scattering distance.
[c] $\Delta\sigma^2$, the change in Debye–Waller factor.
[d] ΔE, the edge energy relative to the model compound.
[e] R^2, the sum of the residuals-squared.
[f] One-atom fit.

are different for different heteropolyanions) led to r(Mn—O) = 1.88 Å, which is 0.25 Å shorter than that of $ZnW_{11}Mn^{II}$. The differences of average bond length can also be observed from the peak positions of the Fourier transform curves (in Fig. 2). Further analysis with two-atom fits proceeded in two stages (1 : 5 fits and 2 : 4 fits) and four models. In models A and B of stage one, two Mn—O distances were refined with n fixed at 5 and 1; in A the unique scatterer was assumed to be closer than the other five, in B it was assumed to be further away. In models C and D of stage two, two Mn—O distances were refined with n fixed at 4 and 2; in C two axial Mn—O bonds were assumed to be shorter than these of equatorial Mn—O bonds; in D they were assumed to be longer. Finally, a three-atom fit was used to determine which of the four equatorial bond lengths in models C and D would best fit model E with n = 1, 1 and 4. No minimum was found for r = 1.92 Å, n = 4, but R^2 decreases for r = 1.86 instead. The results are summarized in Table 5. The longest bond length (2.02 Å) is presumed to be that for the "internal" Mn—O(Zn) bond, since the corresponding average W—O(Zn) distance from the (disordered) crystal structure is 2.191(8) Å. We therefore conclude that the terminal Mn—O bond length is 1.82 Å. We recognize that the k range of the data (3–12) is not sufficient to distinguish the 0.12 Å difference between 1.82 and 1.90 Å in model A, but we can safely rule out the presence of an Mn=O bond ($r \approx 1.7$ Å). The presumed Mn^{IV}—O(H) bond length in the heteropolyanion is similar to that observed for Mn^{IV}—$O(CH_3)$, 1.839 Å, in $Mn(TPP)(OCH_3)_2$ (TPP = tetraphenylporphyrin).[35] An EXAFS investigation of the oxomanganese porphyrin, MnO(TPFPP) [TPFPP = tetrakis(pentafluorophenyl)porphyrin], gave r = 1.67 Å for Mn^{IV}=O.[36]

X-ray absorption edge spectroscopy involves excitation of core electrons to bound states, and reveals substantial chemical and structural information. The positions of the 1*s*–3*d*, 1*s*–4*p* transitions and the absorption threshold have been used to detect changes in oxidation state. The 1*s*–3*d* transition is much weaker in octahedral complexes than in tetrahedral complexes because the former have inversion symmetry. The effective charge of the manganese is therefore mainly reflected in the 1*s*–4*p* and absorption threshold positions (Figs 10 and 11). The latter is determined as the main peak of the first derivative spectrum.

The 1*s*–3*d* transitions for $XW_{11}Mn^{IV}$, $XW_{11}Mn^{III}$ and $XW_{11}Mn^{II}$ (X = P, Si, B and Zn) are very weak, consistent with an octahedral environment for manganese. The positions of the 1*s*–4*p* transition vary significantly, with those for $XW_{11}Mn^{IV}$ being

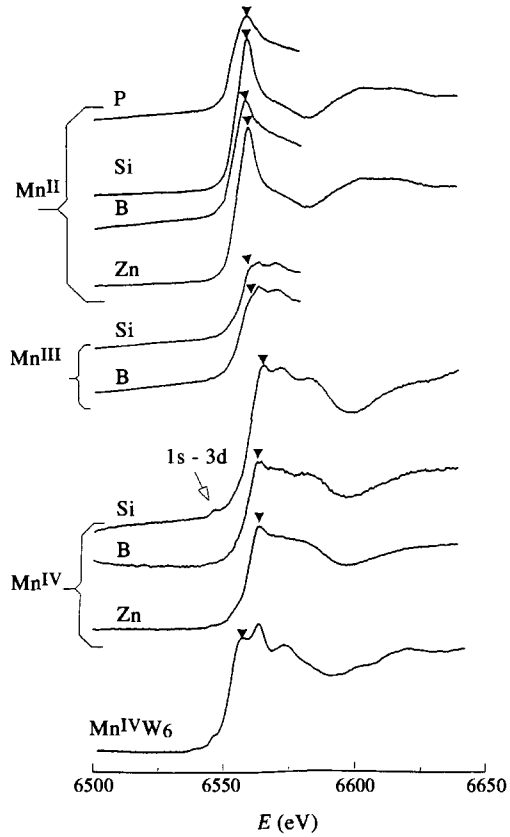

Fig. 10. X-ray fluorescence data for $XW_{11}Mn$ (X = P, Si, B and Zn) and $K_6Na_2[W_6Mn^{IV}O_{24}]\cdot nH_2O$. Positions of the 1*s*–4*p* transitions are indicated by the arrows.

1.5–2.5 eV higher than for $XW_{11}Mn^{III}$, and 3.5–6.0 eV higher than for $XW_{11}Mn^{II}$. The edge shifts (Table 6) and the peak profiles correlate very well with manganese oxidation state.[37] These data provide further evidence for manganese(IV) in the new heteropoly complexes.

FINAL REMARKS

Earlier work has shown that, in aqueous solutions, the $Mn^{II/III}$ redox potentials in these heteropolytungstates are dependent upon the central atom and/or overall anion charge.[17a] In the present investigation we have noted that the separation between the II/III and III/IV couples decreases as the anion charge increases (oxidation state of the central atom decreases). It is therefore not unexpected, given the $Mn^{III/IV}$ potential of 1.10 V for $SiW_{11}Mn$, that no oxidation of $PW_{11}Mn^{III}$ could be observed, although it is of course possible that $PW_{11}Mn^{IV}$ is involved as an intermediate in alkane and alkene oxidations.[7] We shall describe the oxidative reactivity of the characterized $XW_{11}Mn^{IV}$ complexes in a forthcoming paper.

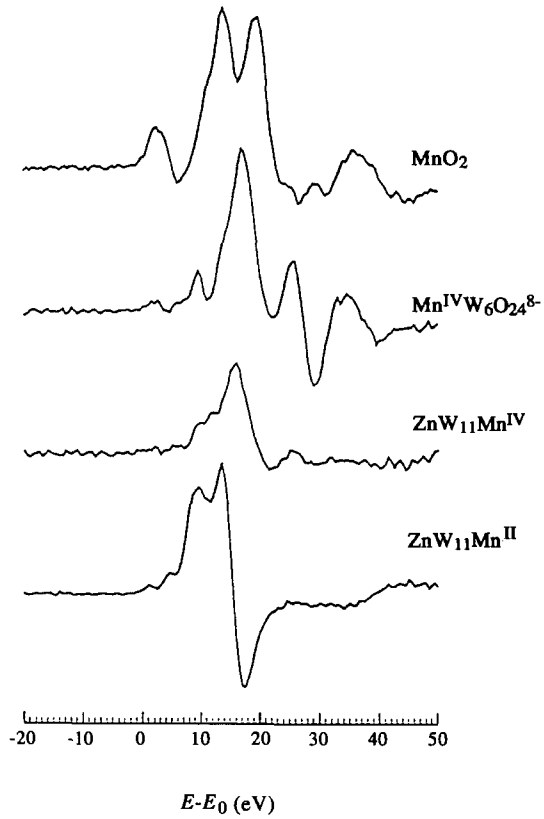

Fig. 11. First derivatives of X-ray fluorescence edge data for selected compounds.

Supplementary material—Atomic coordinates can be obtained from the Cambridge Crystallographic Data Centre.

Table 6. X-ray fluorescence manganese shifts and 1*s*–4*p* transitions for MnO_2, $Na_2K_6[W_6Mn^{IV}O_{24}]\cdot nH_2O$, $Na_7[Mn^{IV}(HIO_6)(H_2IO_6)_2]\cdot nH_2O$ and $XW_{11}Mn^m$ (X = P, Si, B and Zn; *m* = II, III and IV)

Compound	Formal charge on Mn	Mn edge shift $E-E_0$ (eV)[a]	1*s*–4*p* transition (eV)
MnO_2[b]	+4	20.0	6561.5
$[Mn^{IV}W_6O_{24}]^{8-}$	+4	17.0	6559.5
$[Mn^{IV}(H_xIO_6)_3]^{7-}$	+4	17.5	6561.0
$ZnW_{11}Mn^{IV}$	+4	17.0	6559.0
$BW_{11}Mn^{IV}$	+4	19.0	6559.0
$SiW_{11}Mn^{IV}$	+4	17.5	6559.0
$BW_{11}Mn^{III}$	+3	12.5	6555.5
$SiW_{11}Mn^{III}$	+3	13.5	6555.5
$ZnW_{11}Mn^{II}$	+2	12.5	6553.0
$BW_{11}Mn^{II}$	+2	10.0	6553.0
$SiW_{11}Mn^{II}$	+2	11.5	6553.5
$PW_{11}Mn^{II}$	+2	11.5	6554.0

[a] E_0 = 6539 eV from manganese metal.
[b] Pyrolusite.

Acknowledgements—This research has been supported by NSF through Grant No. CHE-9215228. EXAFS and XANES measurements were made at the National Synchrotron Light Source at Brookhaven National Laboratory through Grant No. P41RR01633-11 (to M.T.P.). We thank Dr Michael Wirt and Dr Irit Sagi for technical assistance. Magnetic measurements were made at the Catholic University, Washington, DC by Professor G. Brewer. We are also grateful to Dr John White, Smithsonian Institution, for a sample of pyrolusite.

REFERENCES

1. For recent reviews of this chemistry, see contributions from several authors in *Polyoxometalates: From Platonic Solids to Anti-retroviral Activity* (Edited by M. T. Pope and A. Müller). Kluwer, Dordrecht (1994).
2. Y. Izumi, K. Urabe and M. Onaka, *Zeolite, Clay, and Heteropoly Acid in Organic Reactions*. Kodansha, Tokyo and VCH, New York (1992).
3. D. E. Katsoulis and M. T. Pope, *J. Am. Chem. Soc.* 1984, **106**, 2737.
4. S. P. Harmalker and M. T. Pope, *J. Inorg. Biochem.* 1986, **28**, 85.
5. D. E. Katsoulis and M. T. Pope, *J. Chem. Soc., Chem. Commun.* 1986, **15**, 1186.
6. M. Faraj and C. L. Hill, *J. Chem. Soc., Chem. Commun.* 1987, 1487.
7. C. L. Hill and R. B Brown Jr., *J. Am. Chem. Soc.* 1986, **108**, 536.
8. D. E. Katsoulis, V. S. Tausch and M. T. Pope, *Inorg. Chem.* 1987, **26**, 215.
9. D. E. Katsoulis and M. T. Pope, *J. Chem. Soc., Dalton Trans.* 1989, **8**, 1483.
10. R. Neumann and C. Abu-Gnim, *J. Chem. Soc., Chem. Commun.* 1989, 1324.
11. R. Neumann and C. Abu-Gnim, *J. Am. Chem. Soc.* 1990, **112**, 6025.
12. D. K. Lyon, W. K. Miller, T. Novet, P. J. Domaille, E. Evitt, D. C. Johnson and R. G. Finke, *J. Am. Chem. Soc.* 1991, **113**, 7209.
13. D. Mansuy, J. F. Bartoli, P. Battioni, D. K. Lyon and R. G. Finke, *J. Am. Chem. Soc.* 1991, **113**, 7222.
14. A. M. Khenkin and C. L. Hill, *J. Am. Chem. Soc.* 1993, **115**, 8178 and cited papers.
15. R. Neumann, Private communication (1994).
16. J. F. Liu, Private communication (1993).
17. (a) C. M. Tourné, G. F. Tourné, S. A. Malik and T. J. R. Weakley, *Inorg. Nucl. Chem.* 1970, **32**, 3875; (b) C. M. Tourné and G. F. Tourné, *Bull. Soc. Chim. Fr.* 1969, 1124.
18. J. C. T. Waugh, D. P. Shoemaker and L. Pauling, *Acta Cryst.* 1954, **7**, 438.
19. V. S. Sergienko, V. N. Molchanov, M. A. Porai-Koshits and E. A. Torchenkova, *Koord. Khim.* 1979, **5**, 936.
20. (a) A. Kobayashi, and Y. Sasaki, *Chem. Lett.* 1975,

1123; (b) K. Nagai, Y. Sasaki and M. T. Pope, *J. Am. Chem. Soc.* 1989, **111**, 586.
21. C. M. Flynn and G. D. Stuckey, *Inorg. Chem.* 1969, **8**, 335.
22. K. Wieghardt, U. Bossek, B. Nuber, J. Weiss, J. Bonvoisin, M. Corbella, S. E. Vitols and J. J. Girerd, *J. Am. Chem. Soc.* 1988, **110**, 7399.
23. J. F. Liu, F. Ortéga and M. T. Pope, *J. Chem. Soc., Dalton Trans.* 1992, 1901.
24. (a) B. Dawson, *Acta Cryst.* 1953, **6**, 113; (b) A. Tézé, *J. Inorg. Nucl. Chem.* 1977, **39**, 999.
25. L. S. Powers, B. Chance, Y. Ching and P. Angioillo, *Biophys. J.* 1981, **34**, 465.
26. W. Levason, M. D. Spicer and M. Webster, *Inorg. Chem.* 1992, **31**, 2575.
27. D. M. Wirt, I. Sagi, E. Chen, S. M. Frisbie, R. Lee and M. R. Chance, *J. Am. Chem. Soc.* 1991, **113**, 5299.
28. (a) C. T. Brewer, G. Brewer, L. May, J. Sitar and R. Wang, *J. Chem. Soc., Dalton Trans.* 1993, 151; (b) E. Sinn and C. J. O'Connor, *Inorg. Chim. Acta* 1979, **32**, 29.
29. D. E. Katsoulis, Ph.D. Thesis, Georgetown University (1985).
30. (a) E. Pederson and H. Toflund, *Inorg. Chem.* 1974, **13**, 1603; (b) J. C. Hemper, L. O. Morgan and W. B. Lewis, *Inorg. Chem.* 1970, **9**, 2064;(c) L. S. Singer, *J. Chem. Phys.* 1955, **23**, 379.
31. S. M. Saadeh, M. S. Lah and V. L. Pecoraro, *Inorg. Chem.* 1991, **30**, 8.
32. M. T. Pope, *Heteropoly and Isopoly Oxometalates.* Springer, New York (1983).
33. B. K. Teo and D. C. Joy, *EXAFS Spectroscopy, Techniques and Applications*, pp. 81–85. Springer, New York (1981).
34. R. D. Shannon, *Acta Cryst.* 1976, **A32**, 751.
35. M. J. Camenzind, F. J. Hollander and C. L. Hill, *Inorg. Chem.* 1982, **21**, 4301.
36. M. Schappacher and R. Weiss, *Inorg. Chem.* 1987, **26**, 1190.
37. M. Belli, A. Scafati, A. Bianconi, S. Mobilio, L. Palladino, A. Reale and E. Burattini, *Solid State Commun.* 1980, **35**, 355.